Journal of Molecular Structure 1244 (2021) 130989

Contents lists available at ScienceDirect

Journal of Molecular Structure

journal homepage: www.elsevier.com/locate/molstr

Investigation of spectroscopic, thermal, and biological properties of Fe^{II}, Co^{II}, Zn^{II}, and Ru^{II} complexes derived from azo dye ligand

Nevin Turan[a], Kenan Buldurun[b], Ragip Adiguzel[c,d,*], Abdülmelik Aras[e], Fikret Turkan[f], Ercan Bursal[g]

[a] Department of Chemistry, Faculty of Arts and Sciences, Muş Alparslan University, Muş, Turkey
[b] Department of Food Processing, Vocational School of Technical Sciences, Muş Alparslan University, Muş, Turkey
[c] Department of Chemistry and Chemical Process Technologies, Vocational School of Tunceli, Munzur University, Tunceli, Turkey
[d] Head of Department of Chemical Technologies in Institute of Graduate Studies, Munzur University, Tunceli, Turkey
[e] Department of Biochemistry, Faculty of Science and Arts, Igdır University, Igdır, Turkey
[f] Health Services Vocational School, Igdır University, Igdır, Turkey
[g] Department of Nursing, Muş Alparslan University, Muş, Turkey

ARTICLE INFO

Article history:
Received 14 May 2021
Revised 24 June 2021
Accepted 25 June 2021
Available online 29 June 2021

Keywords:
Azo dye
Pyrazole
Enzyme inhibition
Antioxidant activity
Metal complexes

ABSTRACT

In this study, the novel azo dye Fe^{II}, Co^{II}, Zn^{II}, and Ru^{II} complexes with an azo dye ligand (L: (*E*)-4-((4-methoxyphenyl)diazenyl)-3-methyl-1*H*-pyrazol-5-amine) were synthesized. The structures of the complexes were characterized by FT-IR, elemental analysis, UV-Vis, mass spectra (Fe^{II} and Co^{II}), NMR spectra (only diamagnetic Zn^{II} and Ru^{II}), thermogravimetric and differential thermal analysis (TGA-DTA). All of the newly synthesized compounds were tested for their biochemical properties, including enzyme inhibitory and antioxidant activities. According to the *in vitro* ABTS, DPPH, CUPRAC, and FRAP antioxidant methods, the ligand and its metal complexes showed close antioxidant activities to the standards (BHA, BHT, ascorbic acid, and α-tocopherol). Enzyme inhibitions of the metal complexes were investigated against glutathione S-transferase (GST), acetylcholinesterase (AChE), and butyrylcholinesterase (BChE) enzymes. The best inhibition values (K_i) were observed for Ru(II) complex against GST (14.36 ± 2.16 μM), AChE (16.86 ± 2.74 μM), and BChE (14.12 ± 2.04 μM).

1. Introduction

The azo dyes that are used in lots of diverse areas have good fastness and high dyeing strength properties. They have absorption characteristics, antimicrobial activity, molecular structure, and nonlinear optic. In the literature is encountered the investigation on frontier molecule optical properties of the azo dyes [1].

In previous years, the synthesis and characterization of some transition metal complexes of azo dye ligands (4-(*o*/*p*-substitutedphenylazo)-1H-pyrazole-3,5-diamine) which containing two amine groups on pyrazole ring were studied [2–4]. In addition, the mixed ligand complexes were synthesized from aqua saccharinate Mn(II), Co(II), Cu(II) and Cd(II) complexes and some azo dye ligands (5-methyl-4-(*p*-substituted phenylazo)-2H-pyrazole-3-ylamine) that bearing an amine group on pyrazole ring. These mixed ligand complexes were found to have significantly antioxidant and antimicrobial activity [5,6].

Acetylcholinesterase (AChE) and butyrylcholinesterase (BChE) enzymes catalyze the hydrolysis of the acetylcholine and butyrylcholine that are located at synaptic areas in the central and peripheral nervous systems [7]. AChE inhibitors are used in the treatment of Alzheimer's disease (AD) and some other neurodegenerative diseases [8]. Some former studies reported the reducing symptoms of AD by keeping acetylcholine as a neurotransmitter [9,10].

Glutathione S-transferase (GST) enzyme family members have various metabolic functions such as regulation of the synthesis of certain molecules and the detoxification of xenobiotics, peroxides, and heavy metals [11]. GST has a significant role in promoting the formation of pulmonary fibrosis. A recent study demonstrated that the level of intracellular GST increased in the pulmonary fibrosis cells and the inhibitors of GST can reduce the severity of pulmonary fibrosis in mice models [12]. Therefore, GST inhibitors have crucial functions on the homeostatic regulations [13].

Numerous studies have been performed on the synthesis, and biological properties, of thiophene and pyrazole derivatives [14]. In

* Corresponding author at: Department of Chemistry and Chemical Process Technologies, Vocational School of Tunceli, Munzur University, Tunceli, Turkey.
E-mail address: adiguzelragip@gmail.com (R. Adiguzel).

https://doi.org/10.1016/j.molstruc.2021.130989
0022-2860/

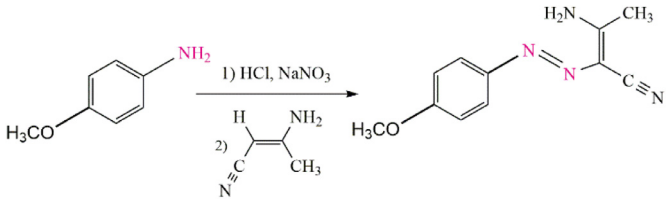

Schema 1. . Coupling reaction in the obtaining of the ligand (L).

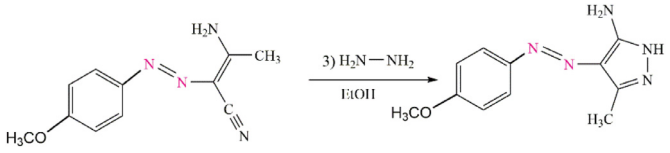

Schema 2. Ring closure reaction in the obtaining of the ligand (L).

the present study, we synthesized a new series of pyrazole derivatives and evaluated their enzyme inhibitory and antioxidant activities.

2. Experimental section

2.1. Materials and measurements

All used solvents were of analytical grade and no further purifications were performed. The metal salts $CoCl_2 \bullet 6H_2O$, $FeCl_2 \bullet 4H_2O$, $ZnCl_2$, and $[RuCl_2(p\text{-cymene})]_2$ and starting materials for the ligand were purchased from Merck, Aldrich, and Alfa Aesar. Elemental analyses were carried out with a Leco CHNS-O model 932 elemental analyzer. FT-IR spectra were recorded with a Perkin Elmer Precisely Spectrum One spectrometer using KBr discs in the wavenumber range of 4000–400 cm^{-1}. Electronic spectral studies were conducted with a Shimadzu model UV-1800 Spectrophotometer in the wavelength 1100–200 nm. Magnetic susceptibility measurements were carried out using the standart Gouy tube technique to $Hg[Co(SCN)_4]$ as a calibrator/calibration. ^1H NMR and ^{13}C NMR data were obtained in DMSO-d_6 solvent on a Bruker AVANCE 400 spectrometer at room temperature. The high-resolution mass spectra (HRMS) were obtained on a Waters LCT Premier XE Mass Spectrometer also coupled to an EQUITY Ultra Performance Liquid Chromatography System. Thermogravimetric analysis (TGA) and differential thermal analysis (DTA) were carried out in a nitrogen atmosphere with a heating rate of 10 °C/min. using Shimadzu DTG-60 AH (Shimadzu DSC 60 A) thermal analyzers. A sample size of 5–10 mg was used and sintered α-alumina was used as the reference material.

2.2. Synthesis and characterization of azo dye ligand (L) and its Fe^{II}, Co^{II}, Zn^{II}, and Ru^{II} complexes

The azo dye ligand was obtained according to the literature method given at **Schema 1 and 2** [15,16]. In course of the synthesis of an azo dye, the ligand has been occurred by azo coupling and ring closure reactions.

Characterization of ligand: FW: 231.25 g/mol. Anal. Calcd. for $C_{11}H_{13}N_5O$: C; 57.13, H; 5.66, N; 30.27. Found: C; 57.10, H; 5.60, N; 30.20. ^1H NMR (DMSO-d_6, 400 MHz) δ 12.00 (s, 1H, N*H*), 7.10–6.90 (m, 4H, Ar-*H*), 6.51 (s, 2H, NH_2), 3.83 (s, 3H, OCH_3), 2.34 (s, 3H, CH_3). ^{13}C NMR (DMSO-d_6, 100 MHz) δ 157.01–140.10 (pyrazole ring), 130.80–114.10 (Ar-*C*), 55.60 (OCH_3), 10.90 (*C*H_3). IR (KBr, cm^{-1}) ν: 3468 (NH), 3357 $(NH_2)_{broad}$, 3180 (Ar-CH), 2967 (Alip.-CH), 1599 (N=N), 1583 (pyrazole C=C) shoulder and overlapped with N=N band, 1536 (C=N), 1498, 1454, 1428 (Ar-C=C), 1396, 1236 (C-N), 1025 (=N-NH-), 796 (δ: NH). UV-Vis (in EtOH): λ max (ε, L mol^{-1} cm^{-1}) 220 (486), 236 (596), 364 (688) nm. Color: Yellow.

Azo dye ligand (L) (0.5 g 2.16 mmol) was dissolved in ethanol (15 mL). $FeCl_2 \bullet 4H_2O$, $CoCl_2 \bullet 6H_2O$, $ZnCl_2$ and $[RuCl_2(p\text{-cymene})]_2$ (0.43 g; 2.16 mmol, 0.514 g; 2.16 mmol, 0.29 g; 2.16 mmol, 0.66 g; 1.08 mmol, respectively) dissolved in ethanol (10 mL) were added. The reaction was refluxed for 4 h. The reaction was completed, following the formation of the reaction with TLC. The solvent was removed. The precipitate formed was filtered, washed with diethyl ether, and dried under vacuum. The product obtained was crystallized in a methanol-dichloromethane (1/2) mixture (Fig. 4).

$[FeLCl_2(H_2O)_2]$: Yield: 82%. FW: 393.75 g/mol. μ_{eff} (B.M.): 4.85. Anal. Calc. for $C_{11}H_{17}N_5O_3FeCl_2$: C; 33.53, H; 4,32, N; 17.76. Found: C; 33.91, H; 4.81, N; 17.81. Selected IR data (KBr, cm^{-1}): ν: 3438 (NH), 3321, 3207 $(NH_2)_{broad}$, 3168 (Ar-CH), 2960 (Alip.-CH), 1643 (pyrazole C=C), 1596 (N=N), 1539 (C=N), 1502, 1469, 1429 (Ar-C=C), 1402, 1245 (C-N), 1029 (=N-NH-) and (δ:NH) band is hidden due to broad bands between 815–684 cm^{-1}, 815 (M-OH_2), 526 ν(M-N), 484 ν(M-O). UV-Vis. (in EtOH): λ max (ε, L mol^{-1} cm^{-1}) 209 (952), 213 (190), 227 (572), 236 (571), 243 (952), 255 (1496), 381 (976), 708 (44) nm. MS [ES]: m/z 393.75 (calc.), 393.30 (found) $[M]^+$. Color: Brownish yellow.

$[CoLCl_2(H_2O)_2] \bullet 1.5H_2O$: Yield: 80%. FW: 424.14 g/mol. μ_{eff} (B.M.): 3.93. Anal. Calc. for $C_{11}H_{20}N_5O_{4.5}CoCl_2$: C; 31.15, H; 4.75, N; 16.51. Found: C; 31.28, H; 4.49, N; 16.63. Selected IR data (KBr, cm^{-1}) ν: 3433 (NH), 3320, 3231 $(NH_2)_{broad}$, 3134, 3096 (Ar-CH), 2963 (Alip.-CH), 1597 (N=N), 1587 (pyrazole C=C), 1539 (C=N), 1500, 1456, 1434 (Ar-C=C), 1403, 1247 (C-N), 1027 (=N-NH-), 815 (M-OH_2), 781 (δ: NH), 573, 527 (M-N), 455 (M-O). UV-Vis. (in EtOH): λ max, nm (ε, L mol^{-1} cm^{-1}) 220 (100), 243 (190), 262, 289, 296 (4000), 305, 321, 351, 361, 382, 399 (4000), 412 (4000), 429 (3818), 434 (3762), 452 (3761), 615 (76), 678 (117) nm. MS [ES]: m/z 427.14 (calc.), 427.37 (^{37}Cl isotopic peak) (found) $[M+2]^+$. Color: Brownish yellow.

$[ZnLCl\ (H_2O)] \bullet Cl \bullet H_2O$: Yield: 76%. FW: 403.29 g/mol. μ_{eff} (B.M.): Dia. Anal. Calc. for $C_{11}H_{17}N_5O_3ZnCl_2$: C; 32.75, H; 4.25 N; 17.35. Found: C; 32.55, H; 4.45, N; 17.05. ^1H NMR (DMSO-d_6, 400 MHz) δ: 11.81 (s, 2H, N**H**), 7.69–6.96 (m, 4H, Ar-**H**), 3.81, 3.39 (s, 3H, OC**H_3**), 2.52, 2.38 (s, 3H, C**H_3**). ^{13}C NMR (DMSO-d_6, 400 MHz) δ 160.08–147.74 pyrazole ring (**C-C=C**), 122.81–114.67 (Ar-**C**), 55.84, 56.48 (OCH_3), 11.01 (**C**H_3). Selected IR data (KBr, cm^{-1}) ν: 3446 (N-N), 3338, 3214 $(NH_2)_{broad}$, 3132, 3067 (Ar-CH), 2998 (Alip.-CH), 1602 (N=N), 1586 (pyrazole C=C), 1500, 1432 (Ar-C=C), 1551 (C=N), 1406, 1249 (C-N), 1029 (=N-NH-), 817 (M-OH_2), 785 (δ:NH), 567, 529 (M-N), 472 (M-O). UV-Vis. (in EtOH): λ max (ε, L mol^{-1} cm^{-1}) 209 (952), 227 (572), 243 (952), 255 (1496), 275 (269), 381 (676), 686 (42), 708 (77) nm. Color: Orange.

$[RuL(\eta^6\text{-}p\text{-cymene})Cl] \bullet Cl \bullet 0.5H_2O$: Yield: 75%. FW: 545.97 g/mol. μ_{eff} (B.M.): Dia. Anal. Calc. for $C_{21}H_{28}N_5O_{1.5}RuCl_2$: C; 46.15, H; 5.17, N; 12.82. Found: C; 46.35, H; 5.29, N; 12.90. ^1H NMR (DMSO-d_6, 400 MHz) δ (ppm): 11.85 (s, 1H, N***H***), 7.74–7.01 (m, 4H, Ar-***H***), 5.83–5.69 (m, 4H, ***p-cymene ring***), 3.81 (s, 3H, OC**H_3**), 2.86–2.81 (h, 1H, C***H***$(CH_3)_2$), 2.38 (s, 3H, C***H_3***), 1.21–1.18 (d, 6H, HC(C***H_3***)***$_2$***), 2.52 (s, 3H, C***H_3***). ^{13}C NMR (100 MHz, DMSO-d_6) δ (ppm): 159.82, 147.68, 129.38–122.56, 114.33, 106.55, 100.55, 86.74–85.99, 65.36 (*pyrazole ring, benzene ring, p-cymene moiety*), 55.85 (O***C***H_3), 40.43 (*p*-cymene ***C***H_3), 30.52 (H***C***$(CH_3)_2$), 24.37, 21.87, 18.34 (HC(***C***$H_3)_2$), 10.80 (***C***H_3). Selected IR data (KBr, cm^{-1}) ν: 3412 (NH), 3280 $(NH_2)_{broad}$, 3059 (Ar-CH), 2961 (Alip.-CH), 1602 (N=N), 1529 (C=N), 1500, 1466, 1428 (Ar-C=C), 1401, 1248 (C-N), 1030 (=N-NH), 788 (δ:NH), 487, 465 (Ru-NH_2 and backdonation). UV-Vis (in EtOH): λ max (ε, L mol^{-1} cm^{-1}) 207 (2476), 226 (48), 239 (2095), 259 (4000), 276 (2836), 297 (4000), 304, 322, 345, 363, 383, 392 (4000), 408 (4000), 421 (3775), 427 (3844) nm. Color: Orange.

2.3. Antioxidant methods

In the present study, the ligand and its metal complexes were examined by four *in vitro* antioxidant methods. ABTS (2,2-azino-bis 3-ethylbenzothiazloine-6-sulphonic acid) and DPPH (1,1-diphenyl-2-picrylhydrazyl) methods were used for measuring the radical scavenging capacity. On the other hand, CUPRAC (cupric ion reducing antioxidant capacity) and FRAP (ferric ion reducing antioxidant power) methods were used for measuring the reducing power antioxidant activity.

2.3.1. ABTS assay

Firstly, ABTS radical solution was obtained by the reaction of 2 mM ABTS in pure water with 2.45 mM $K_2S_2O_8$ solution for twelve hours. To get absorbance at 734 nm phosphate buffer concentration (0.1 M, pH 7.4) was diluted. $ABTS^{\bullet+}$ radical scavenging activity was determined by calculating the reduction in sample absorption [17].

2.3.2. DPPH assay

The ethanolic DPPH radical solution (1 mL, 1 mM) was added to 3 mL of the compounds and standard solutions (10–30 mg/mL) and was incubated for 30 min at room temperature. The absorbance was measured at 517 nm. Decreasing absorbance demonstrated DPPH free radical scavenging capacity [18].

2.3.3. CUPRAC assay

The CUPRAC method was applied as detailed previously [19]. Briefly, the different concentrations (10–30 µg/mL) of samples were mixed with 0.25 mL, 10 mM copper(II) chloride solution, 0.25 mL, 7.5 mM neocuproine solution, and 0.25 mL, 1.0 M buffer solution of CH_3COONH_4. Absorbance was measured at 450 nm.

2.3.4. FRAP assay

Briefly, the compounds at different concentrations (10–30 µg/mL), phosphate buffer (2.5 mL, 0.2 M), and $[K_3Fe(CN)_6]$ (2.5 mL, 1%) were prepared. After 20 min incubation at 50 °C, trichloroacetic acid (2.5 mL, 10%), and $FeCl_3$ (0.5 mL, 0.1%) were added to each mixture. Absorbance was recorded at 700 nm [20].

2.4. Enzyme inhibitory activity

Enzyme inhibitory activities of the metal complexes were investigated against glutathione S-transferase (GST), acetylcholinesterase (AChE), and butyrylcholinesterase (BChE) enzymes.

2.4.1. GST inhibition

CDNB (1-chloro 2,4-dinitrobenzene) was used as the substrate for measuring the GST enzyme activity. *In vitro* GST enzyme inhibition effects of the compounds were determined by the reaction of different concentrations (20–100 µM) of the samples in phosphate buffer (pH 6.5), GST enzyme solution (20 mM), and CDNB solution (25 mM). GST enzyme inhibitions of the compounds were analyzed by measuring the absorbance alterations for 3 min at 340 nm [13].

2.4.2. AChE/BChE inhibitions

AChE and BChE inhibitions of the compounds were determined by using acetylthiocholineiodide (AChI) and butyrylcholineiodide (BChI) substrates. Also, 5,5′-dithiobis 2-nitrobenzoic acid (DTNB) reactive was used to measure the AChE/BChE activities of the sample compounds. Briefly, the sample solutions (50–200 μL), Tris-HCl buffer (100 μ L, 1.0 M), and AChE/BChE enzyme solutions (50 μL 5.3 mEU) were mixed and incubated for 10 min at 25 °C to initiate the enzymatic reaction. Then, 50 μL DTNB (0.5 mM) and 50 μL of AChI/BChI were added to the incubated samples. Finally, the absorbance measurements were performed at 412 nm [21].

3. Results and discussion

3.1. IR spectra

IR absorptions of novel Fe^{II}, Co^{II}, Zn^{II}, and Ru^{II} complexes of azo dye ligand that included pyrazole ring with assignments are given in the experimental section. In the IR spectrum of the ligand, the $\nu(NH_2)$ stretching vibration was observed at 3357 cm^{-1} as a broad peak. As for isolated Fe^{II}, Co^{II}, Zn^{II} and Ru^{II} complexes the same vibration bands shifted to lower frequency and were observed between 3338 and 3207 cm^{-1} as asymmetric and symmetric bands [6,22]. The $\delta(NH_2)$ bending vibration that was expected around 1500–1520 $cm^{-1}$was not observed. Otherwise, the out of plane δ(NH) and ν(C-N) stretching frequencies were found out between 788–781 cm^{-1} (to blue shift) and 1152–1155 cm^{-1} (to redshift), respectively [5,23]. In addition, as sharp and intense two bands the C-N stretching modes that shifted to the higher frequency observed between 1401–1406 and 1245–1249 cm^{-1} in IR spectra of all complexes [5,24]. These results can be indicated as strong evidence regarding complexation over N atom of NH_2 group on pyrazole ring. The (C=N) band in the pyrazole ring in the IR spectrum of Fe^{II}, Co^{II}, Zn^{II}, and Ru^{II} complexes was observed as an intense and sharp peak at 1529–1551 cm^{-1} (for free ligand 1536 cm^{-1}), respectively [22]. The shift that belongs to C=N vibration frequencies is shown as a reason for the change in the electron density of the C=N bond on the pyrazole ring. On the other hand, medium intense and sharp peak belong =N-N-H group that observed at 1024 cm^{-1} shifted to higher frequency region and appeared between 1027 and 1030 cm^{-1}. This phenomenon can be connected to the change of electron density in the pyrazole ring. While the -N=N- peak of the diazo group observed at 1599 cm^{-1}, in the IR spectra of Fe^{II} and Co^{II} complexes this medium intense peak that observed between 1596–1597 cm^{-1} shifted to lower frequency region [5]. The same peak for Zn^{II} and Ru^{II} complexes observed at 1602 cm^{-1} in higher wave number unlike iron and cobalt complexes [5]. All of these reasons show the coordination which provided the by N atom of NH_2 group on the pyrazole ring and by N atom of –N=N- moiety on the azo dye with the metal ion. Again, a new peak which appeared at 815 and 817 cm^{-1} in the Fe^{II}, Co^{II}, and Zn^{II} complexes, respectively are indicated coordinated water molecule to the metal ion [25]. Similarly, weak intense a new absorption band which appeared at 526, 573, 527 and 567, 529 cm^{-1}, respectively for Fe^{II}, Co^{II} and Zn^{II} complexes can be attributed to M-N bond [5,25] (487 and 465 cm^{-1} exclusively Ru^{II} complex can be predicated Ru-NH_2, and Ru-η^6-*p*-cymene) [26]. A new absorption band was observed at 484, 455, and 472 cm^{-1}, respectively in the Fe^{II}, Co^{II}, and Zn^{II} complexes can be assigned to M-O bond in the Fe^{II}, Co^{II}, and Zn^{II} complexes [5,27].

3.2. NMR spactra

NMR spectra of Zn^{II} and Ru^{II} the complexes were analyzed in DMSO-d_6. In the ^{1}H NMR spectra, N-H protons for Zn^{II} and Ru^{II} complexes were seen at 11.81, and 11.85 ppm, respectively, as a broad and singlet peak. Although the $\nu(NH_2)$ stretching vibration bands in IR spectra of all complexes were observed, the singlet peak corresponding to its NH_2 protons in NMR spectra of the zinc and ruthenium complexes wasn't found. It is thought that this peak disappeared due to coordinated or hydrate water and the water in DMSO-d_6. This issue is reported in the literature [28]. These prove show that proton is not removed from the NH and NH_2 groups on pyrazole ring. The multiple peaks corresponding to aromatic protons appeared in the range of 7.69–6.96 and 7.79–7.11 ppm in the ^{1}H NMR spectra of Zn^{II} and Ru^{II}, respectively [29]. Again, multiple peaks in Ru^{II} complex, that appeared at 5.83–5.69 ppm are attributable to the characteristic *p*-cymene ring

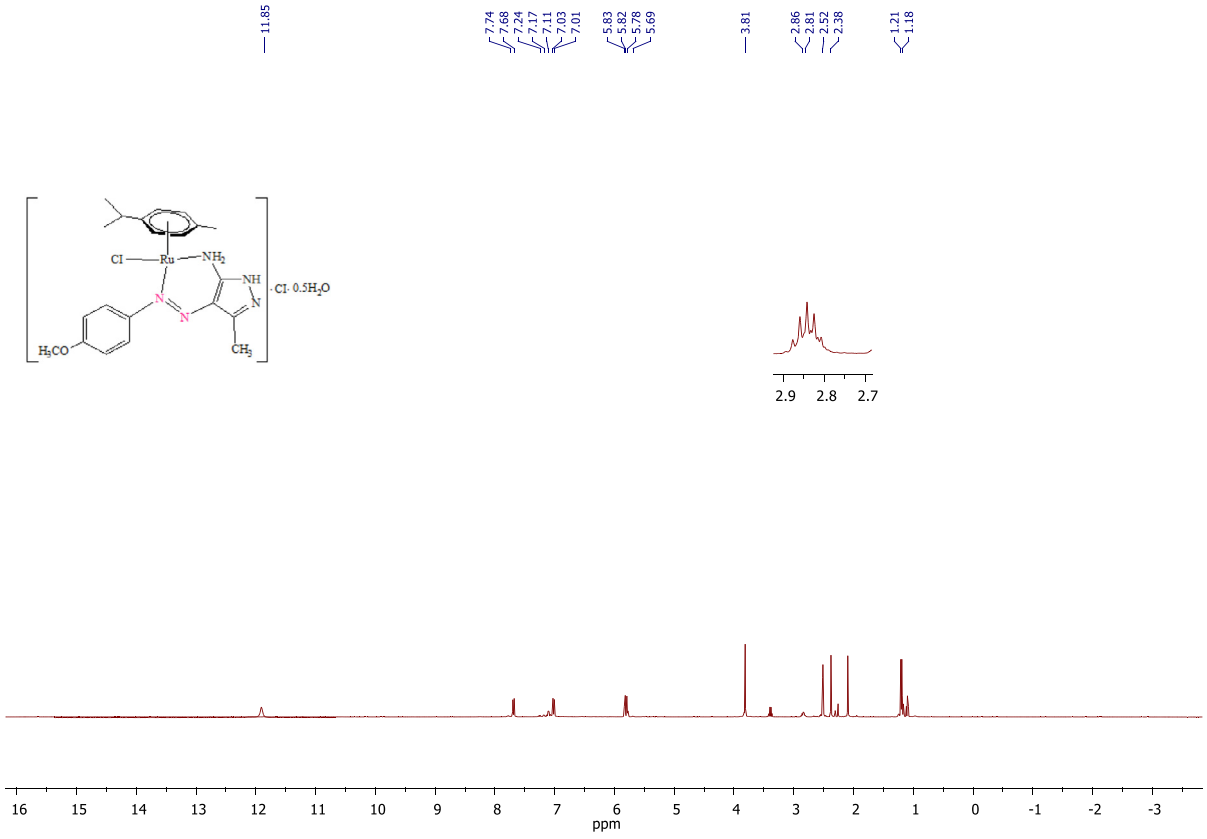

Fig. 1. 1H-NMR spectra of [RuL(η^6-p-cymene)Cl]•Cl•0.5H_2O.

(See Fig. 1) [26,29]. Different from Zn^{II} complex, heptad peaks in the Ru^{II} complex that corresponding to C**H**$(CH_3)_2$ of the *p*-cymene group were observed between 2.86 and 2.81 ppm [26,29].

In the $^{13}C\{^1H\}$ NMR spectra of Zn^{II} complex the carbon peaks belonging to pyrazole ring and aromatic carbons were observed in the range of δ 160.08–147.74 and 122.81–114.67 ppm, respectively [30]. In addition to pyrazole and phenyl ring, including the specific *p*-cymene moiety all peaks related to carbons were seen between 159.82 and 85.99 ppm in Ru^{II} complex [29] (See Fig. 2). For more details of NMR and other spectral analysis data also review the experimental section.

3.3. Mass spectra

The mass spectra of the Fe^{II} and Co^{II} complexes contain peaks attributable to the given molecular ions, m/z 393.30 $[M^+]$ (See Fig. 3) and m/z 427.37 (^{37}Cl isotopic peak) $[M+2]^+$, respectively [31]. The experimental and theoretical mass spectra data of either complex were given in the experimental section. The values that have high abundance in the mass spectra were used as a base. For structural characterization of Zn^{II} and Ru^{II} complexes were used ^1H NMR, ^{13}C NMR, IR spectra, and elemental analysis data.

3.4. Electronic spectra and magnetic properties

The electronic spectra of the ligand and its Fe^{II}, Co^{II}, Zn^{II}, and Ru^{II} complexes were achieved using EtOH solvent in 200–1100 nm. While the ligand showed bands in the 226–236 nm and 364 nm that are responsible for $\pi\rightarrow\pi^*$ and n$\rightarrow\pi^*$ transitions, these bands in Fe^{II} complex shifted to a higher wavelength and were observed at 227–255 nm and 381 nm. In addition, the appeared band at 708 nm mainly ascribed to ligand field d→d transition in octahedral Fe^{II} complex. For the Fe^{II} complex μ_{eff} value was found 4.85 (B.M.). This result has corresponded to a high-spin mononuclear Fe^{II} complex with four unpaired electrons [32]

For the Co^{II} complex the d→d bands, unlike Fe^{II} and Ru^{II} were observed at 615 nm and 678 nm which related to the transitions $^4T_{1g}$ (F)→$^4T_{2g}$ (P), and $^4T_{1g}$ (F)→$^4A_{2g}$ (F), respectively [33]. At the same time, the found μ_{eff} value 3.93 B.M. that are related to three unpaired electrons can be given as evidence to the above results [33].

In the absorption spectra of Zn^{II} belong to $\pi\rightarrow\pi^*$ transition shifted to a higher wavelength and observed at 227–255 nm. On the other hand, the absorption band at 381 nm could be referred to as a charge-transfer transition because the zinc has a d^{10} configuration. When considering the spectrum and the configuration of the Zn^{II} ion, a tetrahedral structure could be supposed for its complexity [34].

The λ_{max} values in the UV spectra of Ru^{II} complex were observed in the region of 259–427 nm. Strong absorption peak that corresponding to $\pi \rightarrow \pi^*$ transition exhibited at 297 nm. Besides, a lower energy broad absorption band that is responsible for metal-to-ligand charge transfer (MLCT) was observed at 408 nm [35].

3.5. TGA-DTA studies

While the weight losses for the complexes of cobalt and zinc occurred in four steps, the losses belong to iron and ruthenium complexes consist of three steps. Generally, in TGA-DTA analyses of synthesized complexes, we discussed the losses of hydrate and a coordinated water molecule, including chlorine losses (See Table 1).

When analyzed TGA curves of all complexes, losses of water molecules of hydration separate from the complexes have been observed in the range of temperature 50–170 °C [25,36]. At the same

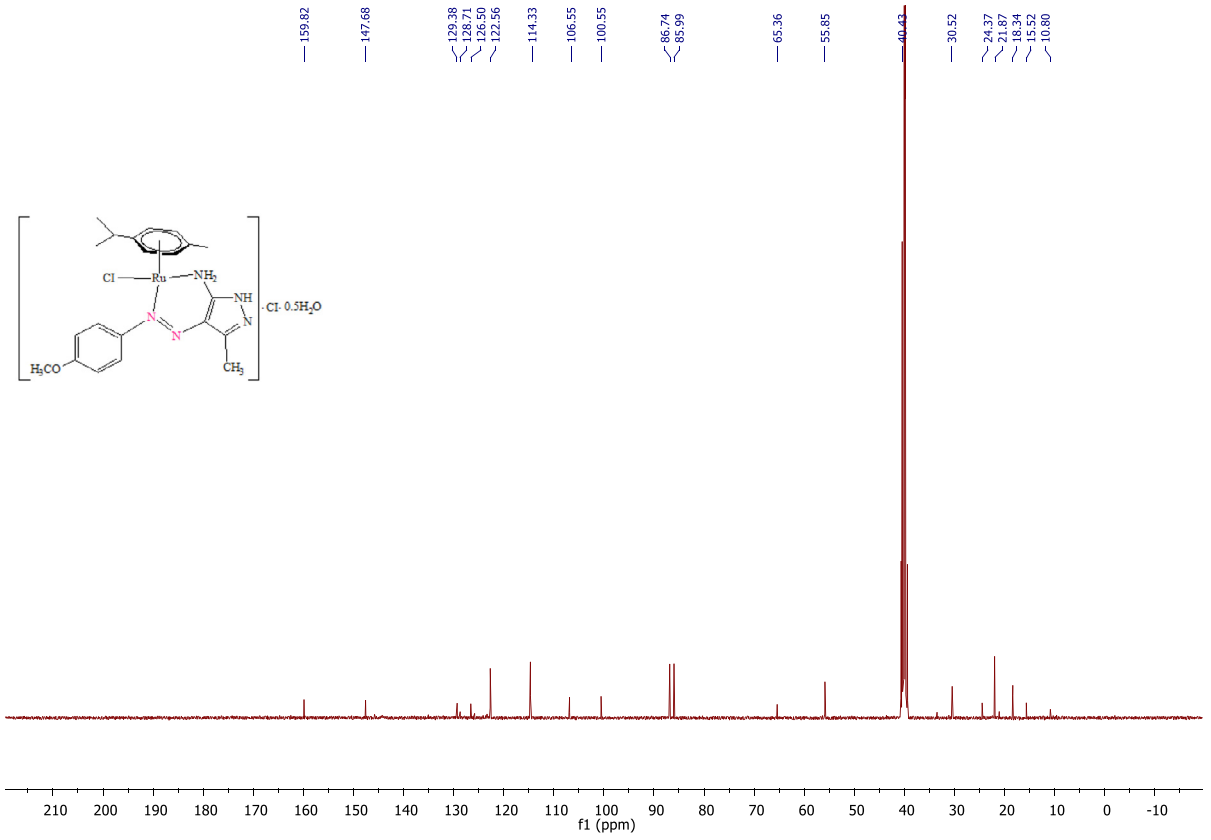

Fig. 2. 13C-NMR spectra of [RuL(η^6-p-cymene)Cl]•Cl•0.5H_2O.

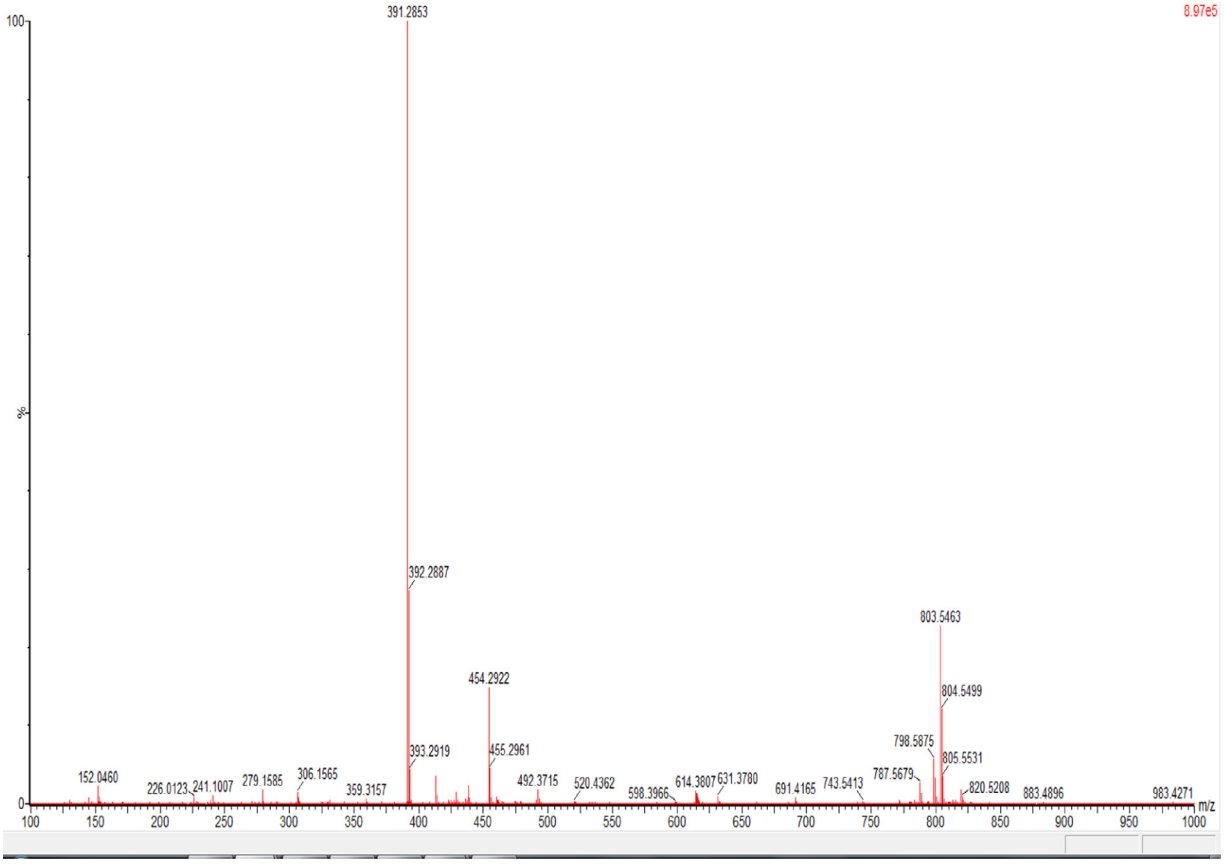

Fig. 3. High-resolution mass spectra (HRMS) for Fe^{II}complex.

Table 1
Proposed decomposition steps and the respective mass losses of complex compounds.

Compounds Molecular weight (g/mol)	Mass loss %, Found (Calc.) Decomposition group				
	First step (°C)	Second step (°C)	Third step (°C)	Fourth step (°C)	
$[FeLCl_2(H_2O)_2]$ 393.75	-	100–253 30.88 (30.96) $2H_2O$ (coord. water), 2Cl, CH_3	253–450 14.10 (15.23) CH_4ON_2	450–800 39.79 (39.61) $C_9H_6N_3$	Residue Fe metal 14.20%
$[CoLCl_2(H_2O)_2]\bullet 1.5H_2O$ 424.14	50.00–170 6.44 (6.36) 1.5 H_2O (hydrate water)	170–300 32.38 (32.27) $2H_2O$ (coord. water), C_2H_6, Cl_2.	300–500 15.42 (15.32) C_3HN_2	500–800 28.32 (28.29) $C_6H_6N_3$	Residue CoO 17.76%
[RuL(η^6-*p*-cymene)Cl]•Cl·$0.5H_2O$ 545.97	50–180 8.68 (8.14) $0.5H_2O$ (hydrate water), Cl.	180–200 24.40 (24.54) $C_{10}H_{14}$	200–450 45.44 (45.32) $C_{11}H_{10}N_5Cl$	-	Residue RuO 22.00%
$[ZnLCl(H_2O)]\bullet Cl\cdot H_2O$ 403.29	50–120 4.48 (4.46) H_2O (hydrate water)	120–210 22.06 (22.04) H_2O (Coord. water), Cl_2	350–530 11.00 (10.91) CH_4N_2	530–800 42.60 (42.40) $C_{10}H_9N_3$	Residue ZnO 15.73%

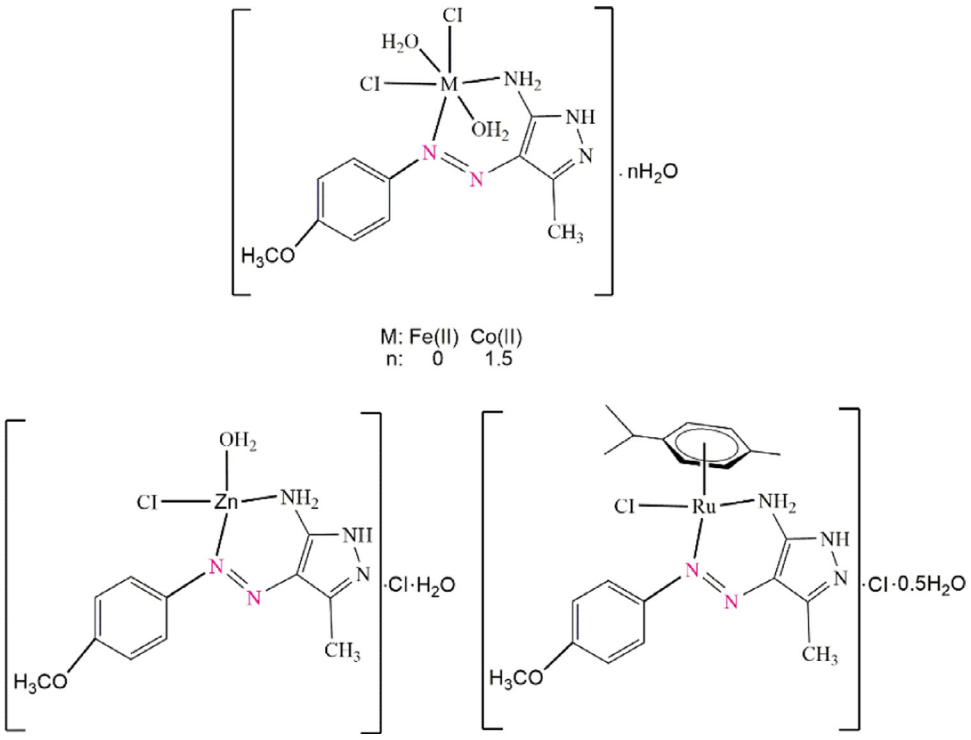

Fig. 4. Proposed structures for Fe^{II}, Co^{II}, Zn^{II}, and Ru^{II}complexes (For interpretation of the references to color in this figure, the reader is referred to the web version of this article). (Both color options are suitable)

time, losses of coordinated water molecules, and chlorine in the complexes have been observed in the range of temperature 120–300 °C [36]. As is expected, according to experimental results and theoretical calculations as a residue in analyses remained metal oxides like CoO, ZnO, RuO except for Fe^{II} complex [25]. In accordance with the results obtained from spectral, elemental, and TGA-DTA analyses, the proposed structures for complexes are given in Fig. 4.

3.6. Antioxidant activity

The antioxidant potentials of the Fe^{II}, Co^{II}, Zn^{II}, and Ru^{II} complexes of the ligand were evaluated by using four well-known *in vitro* spectrophotometric methods, including radical scavenging methods (ABTS and DPPH) and reducing potential methods (FRAP and CUPRAC).

Regarding the ABTS and DPPH radical scavenging methods, decreasing the absorbance of a sample after the reaction process indicates its scavenging antioxidant potential. Absorbance measurements of samples and standards were graphed and presented in Fig. 5.

According to the ABTS results, Co^{II} complex demonstrated an effective cation radical scavenging level like the standards (BHA, BHT, ascorbic acid, and α-tocopherol). The DPPH free radical scavenging level of the Ru^{II} complex was close to the levels of the standards (BHA, BHT, ascorbic acid, and α-tocopherol). However, the DPPH scavenging levels of Fe^{II}, Zn^{II}, and Co^{II} complexes were quite lower

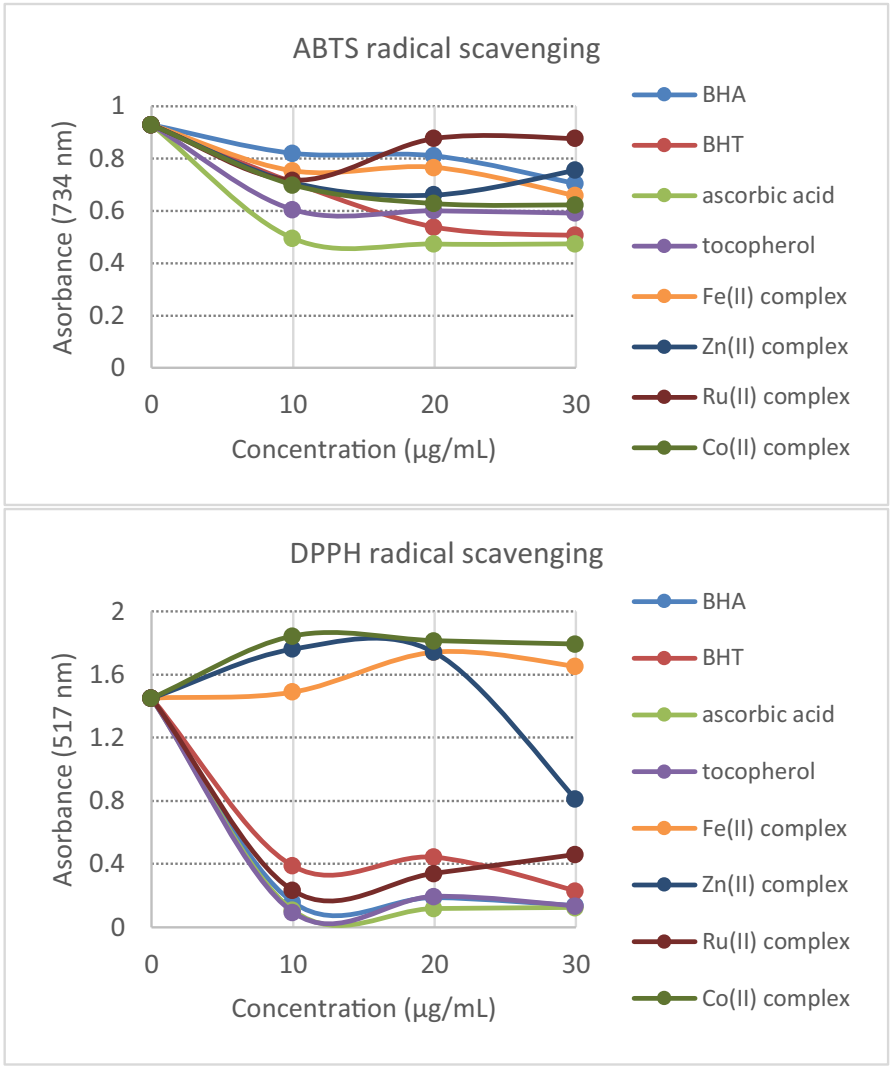

Fig. 5. Radical scavenging antioxidant activities of the complexes and standards by ABTS and DPPH methods.

than the standards. The more effective antioxidant potential of a sample has a lower IC_{50} value (the concentration of a sample for scavenging 50% of radicals). The IC_{50} values of compounds for ABTS and DPPH radical scavenging methods are shown in Table 2.

Regarding the FRAP and CUPRAC methods, increasing absorbance of a sample after the reaction process indicates its reducing potential which means antioxidant potential by single electron transfer. Absorbance measurements of samples and standards were graphed and presented in Fig. 6. According to the CUPRAC results, the Ru^{II} complex demonstrated the highest Cu^{2+} reducing and antioxidant potential among the samples and standards. Likewise, Zn^{II} complex demonstrated the highest Fe^{3+} reducing and antioxidant potential among the samples.

So far, several Schiff bases and their metal complexes have been reported to possess antioxidant activities. The present study has similar results with recent studies on antioxidant activities of different Schiff bases. A recent study reported high DPPH radical scavenging activities of Mn(III), Zn(II), and Pt(II) complexes of a Schiff base [37]. Another study, likewise, reported two copper complexes of a Schiff base had higher DPPH scavenging activities than the standard ascorbic acid [38].

3.7. Enzyme inhibition

The possible disadvantages of multiple-medication in clinical applications such as compliance difficulties and drug-drug interactions and complicated AD nature have prompted the researchers to design novel pharmaceutical ligands against AD [39]. Ligands and their metal complexes have been identified to undergo ligand-substitution reactions with some of the biomolecular structures. Many of them are stated to be used as enzyme inhibitors and have therapeutic potentials [40]. Recently, experiments in the treatment of AD have focused on cholinergic neurotransmission. This process, prompted the evaluation of cholinesterase enzyme inhibitors (ChEIs) that enhance the central cholinergic neurotransmission by inhibiting the degradation of ACh in the brain cells [41].

In this study, the enzyme inhibitions of the Fe^{II}, Zn^{II}, Ru^{II}, and Co^{II} complexes of the ligand against AChE, BChE, and GST enzymes were investigated. The inhibition graphs of compounds were given in supplementary files. The K_i and IC_{50} values were given and the compounds that had the best inhibitions were highlighted in Table 2.

Table 2
IC_{50} and K_i values of the compounds for enzyme inhibitions and antioxidant activities.

Compounds	IC_{50} (μM)								K_i (μM)		
	GST	r^2	AChE	r^2	BChE	r^2	DPPH	ABTS	GST	AChE	BChE
Fe^{II} complex	69.02	0.943	77.39	0.9638	39.57	0.9442	ND	45.0 ± 16.3	43.63 ± 7.01	52.18 ± 8.24	35.87 ± 4.96
Zn^{II} complex	41.02	0.981	85.34	0.976	66.43	0.964	ND	45.3 ± 11.0	16.36 ± 3.26	22.08 ± 5.31	22.36 ± 5.98
Ru^{II} complex	32.45	0.974	38.19	0.9712	33.66	0.975	**13.7 ± 8.0**	155.1 ± 23.5	**14.36 ± 2.16**	**16.86 ± 2.74**	**14.12 ± 2.04**
Co^{II} complex	74.58	0.968	56.42	0.972	88.46	0.967	ND	32.2 ± 12.7	38.12 ± 10.14-	29.58 ± 9.38	44.34 ± 11.39
Tacrine*					7.80	0.9443	-	-			8.77 ± 11.02
BHA	-	-	-	-	-	-	11.2 ± 5.5	61.0 ± 17.8	-	-	-
BHT	-	-	-	-	-	-	13.0 ± 5.6	25.9 ± 6.2	-	-	-
Ascorbic acid	-	-	-	-	-	-	10.9 ± 5.5	20.6 ± 10.0	-	-	-
α-Tocopherol	-	-	-	-	-	-	11.2 ± 5.6	28.0 ± 13.5	-	-	-

* Tacrine was used as a positive control for BChEInhibition effects of newly synthesized complexes of the ligand on AChE, BChE, and GST enzymes were studied. Recently, some enzyme inhibitors such as tacrine, donepezil, huperzine A, galantamine, and rivastigmine compounds have been tested for clinical studies. However, new and more effective inhibitory drug studies are ongoing. The complexes effectively inhibited GST and AChE. Particularly, the GST inhibition value of these compounds was very good. According to the enzyme inhibition methods, a lower K_i value indicates more effective enzyme inhibition of a sample. Considering the K_i values, Ru^{II} complex showed the most effective inhibitions against GST (14.36 ± 2.16 μM), AChE (16.86 ± 2.74 μM), and BChE (14.12 ± 2.04 μM), respectively. On the other hand, the Zn^{II} complex showed the second effective inhibitions against the enzymes. In this research, the enzyme inhibition of the metal complexes was found to have effective inhibitory activities against AChE, BChE, and GST enzymes.

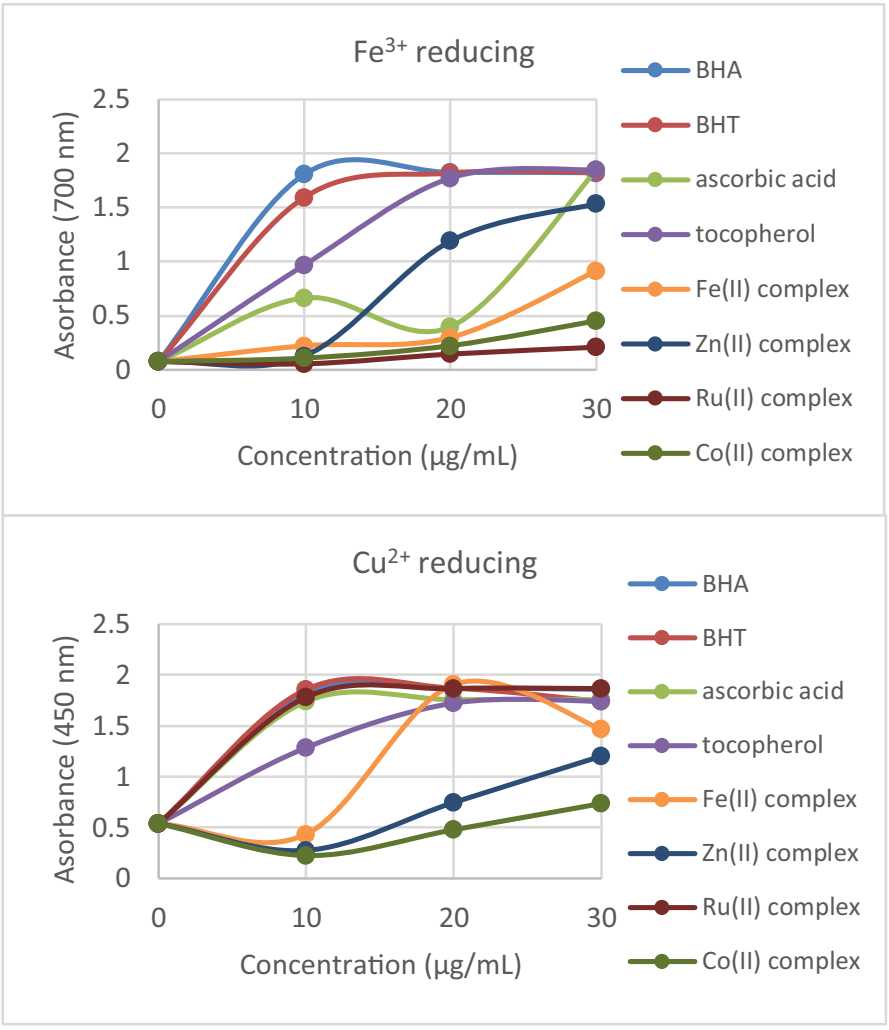

Fig. 6. Reducing antioxidant potentials of the complexes by FRAP and CUPRAC methods.

4. Conclusion

In this study, novel Fe^{II}, Co^{II}, Zn^{II}, and Ru^{II} complexes of azo dye ligand that including diazonium and pyrazole groups were synthesized for bringing to light their several biological activities. The structures of the novel compounds were characterized using UV-Vis spectra, FT-IR, ^{1}H and ^{13}C NMR, magnetic moment, elemental analysis, mass spectra, and TGA analyses. Enzyme inhibition data demonstrated that newly synthesized metal complexes were found to have effective inhibitory activity against the AChE, BChE, and GST enzymes. Surprisingly, for all three used enzymes, Ru^{II} complex was determined as the most effective compound. Also, Zn^{II}

complex had remarkable results against the GST enzyme. We suggest performing more advanced pharmacological tests because results show remarkable activities for Ru^{II} complex against the AChE, BChE, and GST enzymes.

Declaration of Competing Interest

There are no conflicts to declare.

CRediT authorship contribution statement

Nevin Turan: Investigation, Formal analysis, Writing – review & editing, Visualization. **Kenan Buldurun:** Investigation, Formal analysis, Writing – review & editing, Visualization. **Ragip Adiguzel:** Investigation, Formal analysis, Writing – review & editing, Visualization. **Abdülmelik Aras:** Visualization, Supervision, Writing – review & editing. **Fikret Turkan:** Formal analysis, Visualization, Writing – review & editing. **Ercan Bursal:** Visualization, Supervision, Writing – review & editing.

Acknowledgments

We are grateful to Inonu University Catalysis Research and Application Center (for ^{1}H NMR and ^{13}C NMR spectra analyses) and Gazi University Faculty of Pharmacy Department of Pharmaceutical Chemistry (for mass spectra). The enzyme inhibition study was carried out in Igdir University Research Laboratory Application and Research Center (ALUM) in Turkey.

References

[1] B. Çatıkkaş, E. Aktan, E. Yalçın, Vibrational and electronic investigations, NLO, FMO analysis on a hetarylazoindole disperse dye by density functional theory, J. Mol. Struct. 1117 (2016) 218–226.
[2] R. Adiguzel, H. Esener, Z. Ergin, E. Aktan, M. Sekerci, Synthesis and characterization of novel Ni(II), Cu(II) and Cd(II) complexes of 4-(2-chlorphenylazo)-1H-pyrazole-3,5-diamine, Asian J. Chem. 23 (4) (2011) 1846–1850.
[3] R. Adiguzel, H. Esener, Z. Ergin, E. Aktan, N. Turan, M. Sekerci, Synthesis and characterization of Ni(II) and Cd(II) complexes of 4-(4-nitrophenylazo)-1H-pyrazole-3, 5-diamine and 4-(4-methylphenylazo)-1H-pyrazole-3,5-diamine, Asian J. Chem. 23 (6) (2011) 2795–2800.
[4] H. Esener, R. Adiguzel, Z. Ergin, E. Aktan, N. Turan, M. Sekerci, Synthesis and characterization of novel Mn(II), Co(III), Ni(II) and Cd(II) complexes from 4-(2-nitrophenylazo)-1H-pyrazole-3, 5-diamine, Adv. Sci. Lett. 4 (11-12) (2011) 3669–3675.
[5] N. Turan, R. Adigüzel, K. Buldurun, E. Bursal, Spectroscopic, thermal and antioxidant properties of novel mixed ligand-metal complexes obtained from saccharinate complexes and azo dye ligand (mnppa), Int. J. Pharm. 12 (2) (2016) 92–100.
[6] R. Adiguzel, N. Turan, K. Buldurun, H. Korkoca, Spectral, thermal and antimicrobial properties of novel mixed ligand-metal complexes derived from saccharinate complexes and azo dye ligand, Int. J. Pharm. 14 (1) (2018) 9–19.
[7] G. Zengin, K.I. Sinan, G. Ak, M.F. Mahomoodally, M.Y. Paksoy, C. Picot-Allain, J. Glamocilja, M. Sokovic, J. Jekő, Z. Cziáky, Chemical profile, antioxidant, antimicrobial, enzyme inhibitory, and cytotoxicity of seven Apiaceae species from Turkey: a comparative study, Ind. Crop. Prod. 153 (2020) 112572.
[8] F. Türkan, M.N. Atalar, A. Aras, İ. Gülçin, E. Bursal, ICP-MS and HPLC analyses, enzyme inhibition and antioxidant potential of Achillea Schischkinii Sosn, Bioorg. Chem. 94 (2020) 103333.
[9] P. Taslimi, E. Köksal, A.C. Gören, E. Bursal, A. Aras, Ö. Kılıç, S. Alwasel, İ. Gülçin, Anti-alzheimer, antidiabetic and antioxidant potential of satureja cuneifolia and analysis of its phenolic contents by LC-MS/MS, Arab. J. Chem. 13 (3) (2020) 4528–4537.
[10] İ. Gülçin, A.Z. Tel, A.C. Gören, P. Taslimi, S.H. Alwasel, Sage (Salvia pilifera): determination of its polyphenol contents, anticholinergic, antidiabetic and antioxidant activities, J. Food Meas. Charact. 13 (2019) 2062–2074.
[11] J. Gao, B. Chen, H. Lin, Y. Liu, Y. Wei, F. Chen, W. Li, Identification and characterization of the glutathione S-transferase (GST) family in radish reveals a likely role in anthocyanin biosynthesis and heavy metal stress tolerance, Gene 743 (2020) 144484.
[12] N. He, S. Bai, Y. Huang, Y. Xing, L. Chen, F. Yu, C. Lv, Evaluation of glutathione S-transferase inhibition effects on idiopathic pulmonary fibrosis therapy with a near-infrared fluorescent probe in cell and mice models, Anal. Chem. 91 (8) (2019) 5424–5432.
[13] İ. Gulçin, P. Taslimi, A. Aygün, N. Sadeghian, E. Bastem, O.I. Kufrevioglu, F. Turkan, F. Şen, Antidiabetic and antiparasitic potentials: inhibition effects of some natural antioxidant compounds on α-glycosidase, α-amylase and human glutathione S-transferase enzymes, Int. J. Biol. Macromol. 119 (2018) 741–746.
[14] P. Lei, X. Zhang, Y. Xu, G. Xu, X. Liu, X. Yang, X. Zhang, Y. Ling, Synthesis and fungicidal activity of pyrazole derivatives containing 1,2,3,4-tetrahydroquinoline, Chem. Cent. J. 10 (2016) 1–6.
[15] M.H. Elnagdi, M.M.M. Sallam, H.M. Fahmy, S.A.M. Ibrahim, M.A.M. Elias, Reactions with the arylhydrazones of α-cyanoketones: the structure of 2-arylhydrazono-3-ketimino-nitriles, Helv. Chim. Acta 59 (2) (1976) 551–557.
[16] P.C. Tsai, J. Wang, A facile synthesis of some new pyrazolo [1,5-a]pyrimidine heterocyclic disazo dyes and an evaluation of their solvatochromic behaviour, Dye. Pigment. 74 (3) (2007) 578–584.
[17] N. Traverso, R. Ricciarelli, M. Nitti, B. Marengo, A.L. Furfaro, M.A. Pronzato, U.M. Marinari, C. Domenicotti, Role of glutathione in cancer progression and chemoresistance, Oxidative Med. Cell. Longev. 2013 (2013) 972913.
[18] E. Bursal, A. Aras, Ö. Kılıç, Evaluation of antioxidant capacity of endemic plant marrubium astracanicum subsp. Macrodon: identification of its phenolic contents by using HPLC-MS/MS, Nat. Prod. Res. 33 (2019) 1975–1979.
[19] A. Aras, M. Silinsin, M.N. Bingol, E. Bursal, Identification of bioactive polyphenolic compounds and assessment of antioxidant activity of origanum acutidens, Int. Lett. Nat. Sci. 66 (2017) 1–8.
[20] İ. Gulcin, Antioxidants and antioxidant methods: an updated overview, Arch. Toxicol. 94 (2020) 651–715.
[21] M. Işık, Y. Demir, M. Kırıcı, R. Demir, F. Şimşek, Ş. Beydemir, Changes in the anti-oxidant system in adult epilepsy patients receiving anti-epileptic drugs, Arch. Physiol. Biochem. 121 (3) (2015) 97–102.
[22] J. Pons, A. Chadghan, J. Casabó, A. Alvarez-Larena, J.F. Piniella, J. Ros, Cu(II) complexes with pyrazole-derived ligands. Crystal structure of {[diaquanitrato (3-phenyl-5-(2-pyridyl) pyrazole)]copper(II)}nitrate, Polyhedron 20 (19) (2001) 2531–2536.
[23] G.G. Mohamed, N.E. El-Gamel, Structural, spectroscopic and thermal characterization of 2-tert-butylaminomethylpyridine-6-carboxylic acid methylester and its Fe(III), Co(II), Ni(II), Cu(II), Zn(II) and UO_2 (II) complexes, Spectrochim. Acta Part A: Mol. Biomol. Spectrosc. 61 (6) (2005) 1089–1096.
[24] M.S. Masoud, M.F. Amira, A.M. Ramadan, G.M. El-Ashry, Synthesis and characterization of some pyrimidine, purine, amino acid and mixed ligand complexes, Spectrochim. Acta Part A Mol. Biomol. Spectrosc. 69 (1) (2008) 230–238.
[25] M.E. Alkış, K. Buldurun, N. Turan, Y. Alan, Ü.K. Yılmaz, A. Mantarcı, Synthesis, characterization, antiproliferative of pyrimidine based ligand and its Ni(II) and Pd(II) complexes and effectiveness of electroporation, J. Biomol. Struct. Dyn. (2020), doi:10.1080/07391102.2020.1852965.
[26] M.A. Pujante-Galián, S.A. Pérez, M.G. Montalbán, G. Carissimi, M.G. Fuster, G. Víllora, G. García, *p*-Cymene complexes of ruthenium(II) as antitumor agents, Molecules 25 (21) (2020) 5063.
[27] S. Guney, V.T. Yilmaz, W.T. Harrison, Synthesis, crystal structure and properties of trans-$[Cu(sac)_2(en)_2]$ (sac=saccharinato and en=ethylenediamine), J. Coord. Chem. 59 (10) (2006) 1123–1130.
[28] S.K. Mishra, N. Suryaprakash, Intramolecular hydrogen bonding involving organic fluorine: NMR investigations corroborated by DFT-based theoretical calculations, Molecules 22 (3) (2017) 423–466.
[29] R. Adiguzel, F. Türkan, Ü. Yildiko, A. Aras, E. Evren, T. Onkol, Synthesis and in silico studies of novel Ru(II) complexes of Schiff base derivatives of 3-[(4-amino-5-thioxo-1, 2,4-triazole-3-yl)methyl]-2 (3H)-benzoxazolone compounds as potent glutathione S-transferase and cholinesterases inhibitor, J. Mol. Struct. 1231 (2021) 129943.
[30] A.N. Hockstedler, B.A. Edjah, S.Z. Azhar, H. Mendoza, N.A. Brown, H.B. Arrowood, A.C. Clay, A.B. Shah, G.M. Duffek, J. Cui, ^{13}C NMR spectroscopy of heterocycles: 1-phenyl-3-aryl/t-butyl-5-arylpyrazoles, Heterocycl. Commun. 23 (2) (2017) 125–131.
[31] V.G. Dongre, P.P. Karmuse, P.D. Ghugare, M. Gupta, B. Nerurkar, C. Shaha, A. Kumar, Characterization and quantitative determination of impurities in piperaquine phosphate by HPLC and LC/MS/MS, J. Pharm. Biomed. Anal. 43 (1) (2007) 186–195.
[32] K. Buldurun, N. Turan, E. Bursal, A. Mantarcı, F. Turkan, P. Taslimi, İ. Gülçin, Synthesis, spectroscopic properties, crystal structures, antioxidant activities and enzyme inhibition determination of Co (II) and Fe (II) complexes of Schiff base, Res. Chem. Intermed. 46 (1) (2020) 283–297.
[33] C.M. Sharaby, Preparation, characterization and biological activity of Fe(III), Fe(II), Co(II), Ni(II), Cu(II), Zn(II), Cd(II) and UO_2(II) complexes of new cyclodiphosph(V) azane of sulfaguanidine, Spectrochim. Acta Part A Mol. Biomol. Spectrosc. 62 (1-3) (2005) 326–334.
[34] S.S. Konstantinovic, B.C. Radovanovic, Z. Cakic, V.M. Vasić, Synthesis and characterization of Co(II), Ni(II), Cu(II) and Zn(II) complexes with 3-salicylidenehydrazono-2-indolinone, J. Serb. Chem. Soc. 68 (8-9) (2003) 641–647.
[35] B. Sarkar, A. Mondal, Y. Madaan, N. Roy, A. Moorthy, Y.C. Kuo, P. Paira, Luminescent anticancer ruthenium(II)-*p*-cymene complexes of extended imidazophenanthroline ligands: synthesis, structure, reactivity, biomolecular interactions and live cell imaging, Dalton Trans. 48 (32) (2019) 12257–12271.
[36] K. Buldurun, N. Turan, E. Bursal, A. Aras, A. Mantarcı, N. Çolak, F. Türkan, İ. Gülçin, Synthesis, characterization, powder X-ray diffraction analysis, thermal stability, antioxidant properties and enzyme inhibitions of M(II)-Schiff base ligand complexes, J. Biomol. Struct. Dyn. (2020), doi:10.1080/07391102.2020.1802340.

[37] H. Keypour, N. Ansari, M. Mahmoudabadi, R. Karamian, S.H.M. Farida, M.E. Moghadam, R.W. Gable, Mn(III), Zn(II) and Pt(II) macroacyclic complexes: synthesis, X-ray structures, anticancer and antioxidant activities, Inorg. Chim. Acta 509 (2020) 119705–119714.
[38] S.M. El-Medani, A.A. Makhlouf, H. Moustafa, M.A. Afifi, M. Haukka, R.M. Ramadan, Spectroscopic, crystal structural, theoretical and biological studies of phenylacetohydrazide Schiff base derivatives and their copper complexes, J. Mol. Struct. 1208 (2020) 127860.
[39] W. Zheng, J. Li, Z. Qiu, Z. Xia, W. Li, L. Yu, H. Chen, J. Chen, Y. Chen, Z. Hu, Novel bis-(−)-nor-meptazinol derivatives act as dual binding site AChE inhibitors with metal-complexing property, Toxicol. Appl. Pharm. 264 (1) (2012) 65–72.
[40] C.M. Che, F.M. Siu, Metal complexes in medicine with a focus on enzyme inhibition, Curr. Opin. Chem. Biol. 14 (2) (2010) 255–261.
[41] K. Turhan, B. Pektaş, F. Türkan, F.T. Tuğcu, Z. Turgut, P. Taslimi, H.S. Karaman, I. Gulcin, Novel benzo[*b*]xanthene derivatives: bismuth(III) triflate-catalyzed one-pot synthesis, characterization, and acetylcholinesterase, glutathione S–transferase, and butyrylcholinesterase inhibitory properties, Arch. Der Pharm. 353 (2020) e2000030.